Distributed Monitoring of Power System Oscillations Using Multiblock Principal Component Analysis and Higher-order Singular Value Decomposition

Arturo Román-Messina, *Fellow, IEEE*, Alejandro Castillo-Tapia, David A. Román-García,
Marcos A. Hernández-Ortega, *Member, IEEE*, Carlos A. Morales-Rergis, *Member, IEEE*,
and Claudia M. Castro-Arvizu, *Member, IEEE*

Abstract—The primary goal in the analysis of hierarchical distributed monitoring and control architectures is to study the spatiotemporal patterns of the interactions between areas or subsystems. In this paper, a novel conceptual framework for distributed monitoring of power system oscillations using multiblock principal component analysis (MB-PCA) and higher-order singular value decomposition (HOSVD) is proposed to understand, characterize, and visualize the global behavior of the power system. The proposed framework can be used to evaluate the influence of a given area or utility on the oscillatory behavior, uncover low-dimensional structures from high-dimensional data, and analyze the effects of heterogeneous data on the modal characteristics and interpretation of power system. The metrics are then investigated to examine the relationships between the dynamic patterns and participation of individual data blocks in the global behavior of the system. Practical application of these techniques is demonstrated by case studies of two systems: a 14-machine test system and a 5449-bus 635-generator equivalent model of a large power system.

Index Terms—Distributed monitoring, multiblock principal component analysis (MB-PCA), higher-order singular value decomposition (HOSVD), Tucker decomposition.

I. INTRODUCTION

WIDE-AREA monitoring networks consisting of sensors strategically deployed throughout power system

provide a powerful means to observe the system dynamics [1]-[4]. However, the nonuniformity in the locations of the sensors, the growing incorporation of distributed generation, and the use of complementary measurement types, where various key variables are simultaneously monitored at each sensor, pose considerable challenges [5]. Even with simplifications, the resulting models are typically huge, reflecting the global scale and complexity of modern power systems [6]-[8].

The simultaneous distributed analysis of multiple sets of measurements from various geographic regions is essential for various reasons [9]-[11]. Firstly, blocks of variables may provide complementary information of the spatiotemporal behavior of power system. Secondly, a joint analysis of multiple data blocks from interregional systems is needed to find and understand the major patterns and data similarities. Thirdly, the experience with the analysis of large datasets shows that the compression of large multi-dimensional datasets may reveal low-dimensional structures or patterns in the data, primarily because they share one or more oscillation modes.

In this high-order setting, the critical issues include identifying the areas to be monitored, analyzing the associations or relationships between the sets of observed data at various local and global levels, and studying the associated communication and control infrastructures [1], [9]-[12]. Further, local information must be correlated with other regional data concentrators to extract global (inter-utility) information [8]. Additionally, it may be necessary to assess the impacts of heterogeneous generation sources or data types on the dynamic behavior of power system.

In distributed architectures, a power system is divided into blocks of variables associated with various geographic or control areas [3], [9], [13]. As the size and complexity of modern power systems grow and the geographic distribution inherent to renewable generation becomes more prominent across the system, the analysis of spatiotemporal patterns can be more difficult to interpret [9], [13]-[15].

Recently, several approaches for the combined analysis of

massive multivariate datasets have been proposed [3]. Some of these approaches require performing simple concatenation or aggregation of variables, which may overlook the nature of the interactions between subsystems. Another common approach is to use parallel and distributed processing for distributed monitoring and control [1], [14]. Other approaches include multivariate analysis techniques such as multiblock principal component analysis (MB-PCA) [16]-[18], multivariate independent component analysis (ICA) [19], multiway canonical correlation analysis (CCA) [20], [21], and multiblock partial least squares (MB-PLS) [22], [23].

These approaches allow the assessment of impact of a subset of measurements on the global behavior of the power system within the context of distributed oscillation monitoring [9], [10]. As discussed in [1], [14], traditional wide-area monitoring architectures are highly centralized, and it is not easily scalable to incorporate the effect of a massive amount of distributed renewable generation. Distributed monitoring and control architectures using the notion of grid computing are especially promising in providing scalable and flexible solutions to the problem of wide-area oscillation monitoring [14], including data exchange and parallel and distributed processing. Although these approaches address the problem of developing more efficient monitoring schemes, there remains a need to develop techniques that use these data for oscillation monitoring.

In this paper, a novel framework based on MB-PCA and sequentially truncated higher-order singular value decomposition (ST-HOSVD) is proposed to understand, characterize, and visualize the spatiotemporal patterns of oscillatory activity. The proposed framework can be used to evaluate the influence of a given area or utility on the oscillatory behavior, uncover low-dimensional structures from high-dimensional data, and analyze the effects of heterogeneous data on the modal characteristics and interpretation of the power system.

This paper is organized as follows. Section II presents the background and motivation. In Section III, a framework based on MB-PCA is introduced to jointly analyze multiple sets of data. Section IV discusses the use of tensor-based multiblock representations for the monitoring and analysis of large-scale complex systems. Results are presented in Section V for two systems: a 14-machine test system and a 5449-bus 635-generator equivalent model of a large power system. Finally, conclusions are drawn in Section VI.

II. BACKGROUND AND MOTIVATION

A. Hierachical Distributed Monitoring System Architecture

To obtain a conceptual understanding of the adopted model, a hierarchical distributed monitoring system architecture consisting of M areas or zones indexed with $j = 1, 2, ..., M$ is considered. Particular cases may include large clusters of wind or solar photovoltaic farms or microgrids.

A phasor data concentrator (PDC) collects time-stamped measurements stored as blocks of variables evolving with time. A schematic of the hierarchical distributed architecture of the adopted wide-area monitoring system (WAMS) is given in Fig. 1. The solid thick lines correspond to the contribu-

tion of each control area to the super PDC. X_j ($j = 1, 2, ..., M$) is the matrix of local measurements, and Y_j is a subset of measurements or aggregated system behavior used for regression.
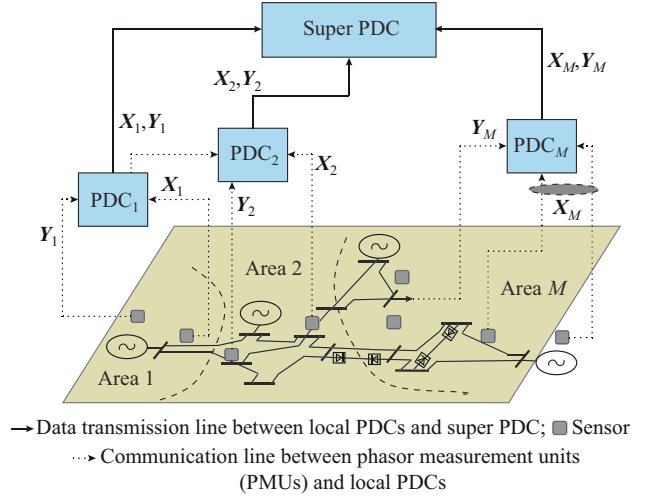

Fig. 1.   Schematic of hierarchical distributed architecture of adopted WAMS.

Throughout this paper, it is assumed that each PDC communicates with neighboring PDCs and the super PDC. Conceptually, the model gives the relationships between the data blocks at the upper (global) level. At the lower level, the model shows the details of each data block [3]. Purely distributed or semidistributed monitoring architectures can also be obtained by the proper interpretation of this model.

To formally introduce the proposed model, consider that area k has a sparse network of m_k sensors deployed to monitor the dynamic behavior of power system. Further, assume that the time evolution of the measured data at sensor j is denoted by $x_j(t_l)$ ($j = 1, 2, ..., m_k$, $l = 1, 2, ..., N$), where N is the number of samples or observations and t is the time. Once a fault is detected, the measured data are transmitted to a local PDC for storage and analysis, as suggested in Fig. 1.

From the above description of the WAMS architecture, the set of local data blocks can be organized into M two-way arrays.

$$X_j(t) = \begin{bmatrix} x_1(t_0) & x_2(t_0) & \dots & x_{m_j}(t_0) \\ x_1(t_1) & x_2(t_1) & \dots & x_{m_j}(t_1) \\ \vdots & \vdots & & \vdots \\ x_1(t_{N-1}) & x_2(t_{N-1}) & \dots & x_{m_j}(t_{N-1}) \end{bmatrix} \in \Re^{N \times m_j}$$

$$j = 1, 2, ..., M \quad (1)$$

Note that each dataset in (1) associated with the M regions may have different numbers of sensors m_j but the same number of observations N.

Following the notation in [3], a multiblock representation can be formed by horizontally concatenating the individual PDC measurements as:

$$X = [X_1 \quad X_2 \quad \dots \quad X_M] \in \Re^{N \times m_t} \quad M \geq 2 \quad (2)$$

where $m_t = m_1 + m_2 + ... + m_M$; and the data blocks X_j ($j = 1, 2, ..., M$) may be of different sizes in general. Moreover, a

response data matrix Y_j, usually used for regression, can be obtained and expressed as:

$$Y=[\,Y_1 \quad Y_2 \quad \ldots \quad Y_M\,]\in \Re^{N\times m_y} \quad M\geq 2 \tag{3}$$

where m_y is the number of output variables selected for regression. $m_y \neq m_t$ in general, as suggested in Fig. 1.

By their very nature, the models in the form of (2) and (3) are large, complex, and heterogeneous in structure, as the data blocks X_j and Y_j may contain different spatiotemporal structures and include heterogeneous data types.

B. Single-block PCA (SB-PCA)

PCA has been extensively used for the wide-area monitoring and data clustering of power systems. Given a set of measurements in the form of (2), SB-PCA finds a new set of variables such that [22]:

$$X=TP^T+E \tag{4}$$

where $T\in\Re^{N\times r}$ is the matrix of principal component (PC) scores, and r is the number of relevant PCs; $P\in\Re^{m_t\times r}$ is the matrix of PC loadings; and E is a residual matrix that is minimized in the least-squares sense.

Equation (4) is equivalent to [24]:

$$X=TP^T+E=\underbrace{\sum_{i=1}^{r}t_i p_i^T}_{\substack{\text{Physically relevant}\\\text{coordinates}}}+\underbrace{\sum_{j=r+1}^{s}t_j p_j^T}_{\substack{\text{Non-physical}\\\text{coordinates}}}=\underbrace{\sum_{i=1}^{r}t_i\otimes p_i}_{TP^T}+E \tag{5}$$

where t_i is the score vector; p_i is the loading vector; and the symbol $\otimes$ denotes the outer product. A similar interpretation is obtained using proper orthogonal decomposition (POD) [24], [25]. In practice, r is chosen such that a few PCs accurately approximate the observational data, and E is chosen to be as small as possible.

Formally, the PCs can be obtained from an eigenvalue analysis of the covariance matrix C:

$$\frac{1}{N-1}Cp_i=\frac{1}{N-1}X^TXp_i=\lambda_i p_i \tag{6}$$

where λ_i is the eigenvalue; and $C=X^TX$ is the correlation matrix. Alternatively, the PCs can be extracted from singular value decomposition (SVD) of the measurement matrix in (2) [25].

Various practical interpretations of this model can be given as follows [26].

1) Each term $t_i p_i^T$ in (5) represents a modal matrix E_i.

2) The score and loading vectors are orthogonal and orthonormal, i.e., $t_i^T t_j=0$ and $p_i p_i^T=1$.

3) The product $t_i p_i^T$ in (5) can be interpreted in terms of the primary matrix products (two-dimensional tensors).

Figure 2 gives a representation of the system model in (5) in terms of the tensor products. The block weights w_i ($i=1,2,…,M$) give the contributions of the block scores T_i to the super-score matrix T in MB-PCA.

Two practical problems arise in the application of SB-PCA approaches. First, these techniques cannot describe the relationships between data blocks, and may be inappropriate for analyzing data interactions. The second limitation concerns the interpretation of results when some data blocks have more variables than others and only provide a partial and somewhat limited view of the global behavior of power
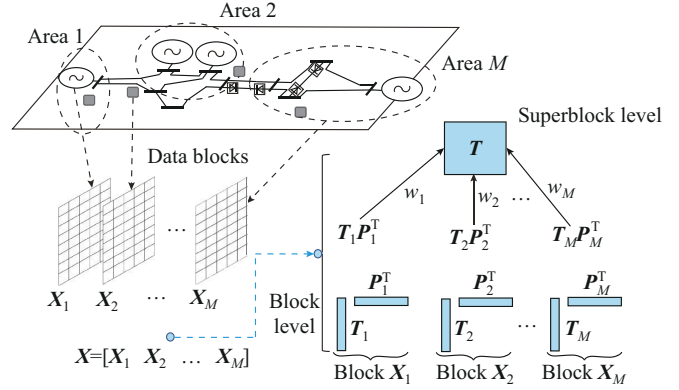
system.

Fig. 2.   Representation of system model in (5) in terms of tensor products.

Several refinements to this technique are discussed next, and a unifying framework to study and characterize inter-system oscillations is provided.

III. FRAMEWORK BASED ON MB-PCA

MB-PCA has recently emerged as a powerful analysis tool for the joint analysis of high-dimensional data [26]-[28]. The adopted MB-PCA framework is introduced in the following subsections, and the critical properties are summarized.

A. Background

As presented in [3], MB-PCA allows a multiblock component model of the following form to be recursively obtained:

$$\begin{cases} X=TP^T+E \\ Y=UQ^T+F \end{cases} \tag{7}$$

where T and U are the matrices of block scores; Y is the response matrix; and P and Q are the loading matrices. The superblock matrix T can then be defined as:

$$T=\sum_{i=1}^{M}w_i X_i \tag{8}$$

Further, $X_i=T_i P_i^T$, and P^T is the loading matrix defined as:

$$P^T=[\,P_1^T \quad P_2^T \quad \ldots \quad P_M^T\,] \tag{9}$$

A similar interpretation can be made for U and Q^T.

The MB-PCA approach seeks correlated consensus directions from the measurement blocks that maximally capture block variations. Mathematically, this is given by the following optimization problem [28]:

$$\begin{cases} \displaystyle\max_{p_1,p_2,…,p_M}\sum_{\substack{i\neq j}}^{M}p_i^T(X_i X_j^T)p_i \\ \text{s.t. } \|p_i\|=1 \end{cases} \tag{10}$$

where $X_i X_j^T$ is the cross-covariance matrix.

Various interpretations of this model are summarized as below.

1) The score and loading vectors satisfy the conditions $t_i^T t_j=0$, $t_i^T t_i=1$, $p_i^T p_j=0$, $p_i^T p_i=1$, $\forall i,j$.

2) As shown in Fig. 2, the block weights w_i give the contribution of each data block to the superblock scores.

3) The residuals provide the information of outlier detection, and can be computed as:

$$E = X - TP^{\mathrm{T}} \tag{11}$$

$$F = Y - UQ^{\mathrm{T}} \tag{12}$$

With these assumptions, two types of metrics are considered: measures of the contribution of a variable to the local area dynamics, and measures of interaction between variables in two or more areas or geographic regions.

In the first case, a practical local interpretation of the contributions of a set of variables to the dynamics of the area can be obtained from the loadings of the data matrices. Let $p_i = [p_{1i}, p_{2i}, ..., p_{m_T i}]^{\mathrm{T}}$ be the loading vector associated with the ith PC.

Intuitively, the normalized contribution C_{ij} from the jth variable to the ith oscillatory mode or PC (a dominance measure) is given by the metric C_{ij}:

$$C_{ij} = \frac{p_{ij}^2}{\sum\limits_{l=1}^{m_k} p_{lj}^2} \quad i = 1, 2, ..., m_T, j = 1, 2, ..., r \tag{13}$$

where p_{ij} is the jth element in p_i. One could also calculate the contribution of a set of variables to the dynamics of the area or the contribution of each block to the global behavior of the system, as explained below.

Alternatively, the relationships between the blocks of variables can be obtained using specialized approaches such as MB-PLS [29] and multiblock CCA (MB-CCA) [30]. The numerical implementation of MB-PCA is firstly discussed.

B. Numerical Implementation of MB-PCA

The MB-PCA algorithm developed in this paper is based on [15], [16] and summarized as follows.

A data matrix of concatenated data blocks, $X = [X_1, X_2, ..., X_M] \in \mathfrak{R}^{N \times m_t}$, $M \geq 2$, is firstly given.

Step 1: normalize, center, and scale the data blocks X_i, $i = 1, 2, ..., M$.

Step 2: select a column of one of the blocks X_i as a starting consensus t_T and iterate until the convergence of t_T.

1) Compute the block variable loadings using regression as $p_i = X_i^{\mathrm{T}} t_T / (t_T^{\mathrm{T}} t_T)$, s.t. $|p_i| = 1$, $i = 1, 2, ..., M$.

2) Compute the block scores as $t_i = X_i p_i$, $i = 1, 2, ..., M$.

3) Combine all block scores into a score superblock $T = [t_1, t_2, ..., t_M]$.

4) Compute the super-weights $w = T^{\mathrm{T}} t_T / (t_T^{\mathrm{T}} t_T)$, $|w| = 1$, with $w = [w_1, w_2, ..., w_M]^{\mathrm{T}}$.

5) Determine the super-scores as $t_i = Tw$. Select a new t_T and return to 1).

Step 3: upon convergence, deflate the residuals as $p_i = X_i^{\mathrm{T}} t_T / (t_T^{\mathrm{T}} t_T)$, $X_i = X_i - t_T p_i^{\mathrm{T}}$.

The variations of this basic procedure are given in [16] and discussed in the application of simulation data.

IV. Tensor-based Multiblock Representations

WAMSs produce data in the form of multi-dimensional arrays that can be represented using tensors.

Two cases are of particular interest in this paper: ① joint analysis of multivariate PMU data such as the bus frequency, the magnitude of the bus voltage and the phase angle, or the active and reactive powers; and ② the data of the same type associated with different contingencies or historical data collected using the same set of sensors. A more general discussion of this issue can be found in [12].

A tensor-based multiblock representation of multivariate PMU data is illustrated in Fig. 3. It is essential to note in this case that the *n*-way arrays in Fig. 3 are unfolded across the sensor dimension as:

$$\hat{X} = \left[\underbrace{X_1^1 \quad X_1^2 \quad ... \quad X_1^{m_1}}_{PDC_1} \quad ... \quad \underbrace{X_M^1 \quad X_M^2 \quad ... \quad X_M^{m_M}}_{PDC_M} \right] \tag{14}$$

where X_j^k ($k = 1, 2, ..., m_j$) is the kth measurement matrix associated with area j. Further, it is observed that each matrix X_j^k can be related to a given measurement type or represent historical data, e.g., a single data type coming from multiple fault scenarios or recorded events.
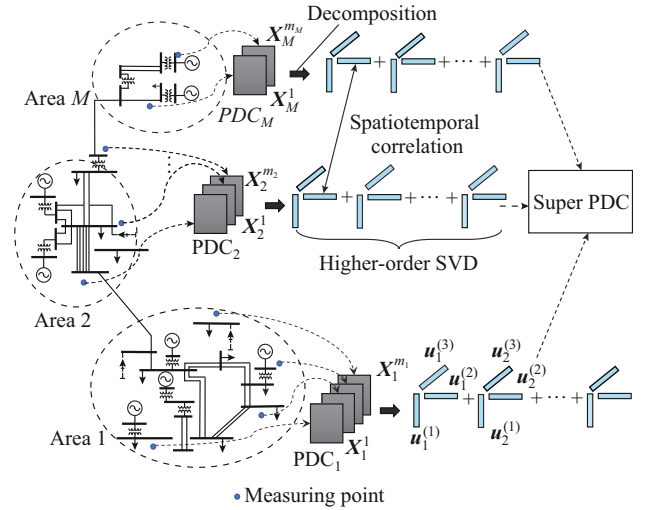

Fig. 3.   Tensor-based multiblock representation of multivariate PMU data.

A. Tucker Decomposition

A more useful representation of multivariate PMU data in (14) can be obtained from tensor decomposition of the set of local data blocks associated with each PDC in Fig. 3. Note that in this case, each slice X_j^k ($j = 1, 2, ..., M$, $k = 1, 2, ..., m_j$) represents a measurement matrix associated with a single data type.

Let χ denote an Nth-order tensor of dimension $\mathfrak{R}^{I_1 \times I_2 \times ... \times I_N}$. Tucker decomposition is a technique that decomposes a third-order tensor χ into a set of three factor matrices, $U^{(1)}$, $U^{(2)}$, and $U^{(3)}$, and a core tensor $S \in \mathfrak{R}^{r_1 \times r_2 \times r_3}$ with $r_i \leq I_i$ [31]-[33]. Mathematically, χ can be numerically estimated by solving the following optimization problem:

$$\min_{\hat{\chi}} f(\hat{\chi}) = \|\chi - \hat{\chi}\|_F^2 \tag{15}$$

where $\hat{\chi}$ is the tensor approximation to χ. The enhancements to this basic formulation are discussed below.

B. HOSVD

HOSVD is a constrained form of Tucker decomposition that ensures the orthogonality of the factor matrices and core tensor [34], [35]. For simplicity and clarity of exposition, a

third-order tensor (two slices in the data blocks in Fig. 3) is considered. Using HOSVD, the third-order tensor $\chi \in \Re^{I_1 \times I_2 \times I_3}$ is decomposed into three factor matrices and a core tensor as:

$$\hat{\chi} = S \times_1 U^{(1)} \times_2 U^{(2)} \times_3 U^{(3)} \qquad (16)$$

where $U^{(i)} = [u_1^{(i)}, u_2^{(i)}, ..., u_{I_i}^{(i)}] \in \Re^{I_i \times I_i}$, $i = 1, 2, 3$ is the orthogonal (factor) matrix, i.e., $(U^{(i)})^T U^{(i)} = I_i$, that form the Tucker factors; $S \in \Re^{I_1 \times I_2 \times I_3}$ is the core tensor; and $\times_n$ $(n = 1, 2, 3)$ denotes the n-mode multiplication of tensors. In this sense, S contains the ith-mode singular values of χ and gives the degree of interaction among the $U^{(i)}$ components.

In physical terms, $U^{(i)}$ can be interpreted as the PCs of each tensor mode, and $U^{(1)}$ gives the spatial shapes or patterns, which allows the derivation of similar measures to those introduced in (13). As a byproduct, an HOSVD analysis of the measurement matrix X and response matrix Y can be used for regression, but this is not discussed in this paper.

As discussed below, the datasets in (2) are usually low-rank and sparse in a reduced subspace in typical system applications. Drawing on this observation, an HOSVD analysis of the array of measurements associated with area k given by the tensor $\chi \in \Re^{m_j \times N \times m_k}$ yields a low-dimensional representation, i.e., a full-rank decomposition, which is expressed as:

$$\hat{\chi} = \hat{S} \times_1 \hat{U}^{(1)} \times_2 \hat{U}^{(2)} \times_3 \hat{U}^{(3)} \qquad (17)$$

where $\hat{S} \in \Re^{r_1 \times r_2 \times r_3}$ is the core tensor for $r_1 \leq m_j$, $r_2 \leq N$, and $r_3 \leq m_k$; and $\hat{U}^{(1)} \in \Re^{m_j \times r_1}$, $\hat{U}^{(2)} \in \Re^{N \times r_2}$, and $\hat{U}^{(3)} \in \Re^{m_k \times r_3}$ are the orthonormal factors.

It can also be demonstrated that (17) admits a spatiotemporal representation of the form (18) or (19):

$$\hat{\chi} = \underbrace{(\hat{S} \times_2 \hat{U}^{(2)} \times_3 \hat{U}^{(3)})}_{G} \times_1 \hat{U}^{(1)} \qquad (18)$$

$$\hat{\chi} = G \times_1 \hat{U}^{(1)} \qquad (19)$$

where $\hat{U}^{(1)} = [\hat{u}_1^{(i)}, \hat{u}_2^{(i)}, ..., \hat{u}_{I_i}^{(i)}]$ is a matrix that contains the spatial patterns (mode shapes or loading matrix P^T in (7)) and provides a common basis for the subspace of measurements associated with (14). The tensor $G = \hat{S} \times_2 \hat{U}^{(2)} \times_3 \hat{U}^{(3)} \in \Re^{r_1 \times N \times m_k}$ contains the temporal patterns or modes of each subspace of measurements, and provides a compressed representation of the block scores in (7) and (8).

However, HOSVD is computationally demanding since the tensor representations are sparse and high-dimensional. As a result, a low-rank approximation is sought such that $\|\chi - \hat{\chi}\| \leq \varepsilon \|\chi\|$, where ε is the desired or specified accuracy.

In the following subsection, ST-HOSVD is explored to assess the dynamic behavior of power system.

C. ST-HOSVD

As noted above, tensors in the applications of dynamics of power systems are usually low-rank. A more efficient algorithm for computing the HOSVD of (15) is the ST-HOSVD approach introduced in [36], [37].

This algorithm enables a low-rank accurate (and faster) HOSVD approximation to be efficiently obtained, in which the tensor ranks are sequentially computed in a greedy way.

For each mode, the ith-rank approximation $r_i \leq I_i$ is determined by performing an SVD of $X^{(i)}$, where r_i is the rank.

In this procedure, the rank r_N is selected in such a way that the singular values σ_i of X_i satisfy [31]:

$$\sum_{j=r_i+1}^{I_i} \left(\sigma_i^j \right)^2 \leq \frac{\varepsilon^2}{N} \|\chi\|^2 \qquad (20)$$

This approach has several advantages over conventional truncated HOSVD approaches, such as faster computation speed, a compressed representation, reduced computational efforts, and the possibility of providing an approximate error analysis.

The ST-HOSVD approach implemented in this paper can be summarized as follows [36], [37].

1) Given a set of measurement data in (2), center and scale the individual data blocks. Construct a multiway array using the tensor slice representations as: $\chi(:,:,i) = \hat{X}_i$, $i = 1, 2, ..., M$, where $\hat{X}_i$ is the scaled data.

2) Set the desired accuracy ε in (20) and compute the ST-HOSVD using the approach in [36].

3) Obtain the core tensor S and factor matrices $U^{(i)}$, $i = 1, 2, 3$.

4) Rank the tensor modes using energy criteria.

5) Compute the ST-HOSVD mode shapes from $\hat{U}^{(1)}$, the ST-HOSVD damping, and the frequency estimates from G.

6) If necessary, reconstruct the selected dynamics using (17) or (19), extract the spatiotemporal features of interest, and visualize the higher-order PCs. Extract the modal properties.

Other potential applications that are actively investigated include sensor placement, anomaly detection, and distributed monitoring.

D. Case Studies

Three case studies representing various degrees of system complexity and modeling are simulated and summarized below to highlight the importance of joint analysis of multivariate datasets.

1) Case 1: the three-way arrays in Fig. 3 are unfolded, and the resulting model is analyzed using MB-PCA or ST-HOSVD.

2) Case 2: the three-way array in (17) is treated as a single three-way tensor, and the spatiotemporal representation is obtained using (16) through (18).

3) Case 3: the three-way data associated with each PDC are individually analyzed, and the local results are combined to obtain a global model of the system.

V. Application of Simulated Data

In this section, the abilities of MB-PCA and HOSVD to extract and characterize spatiotemporal patterns are tested with two systems: a 14-machine test system and a 5449-bus 635-generator equivalent model of a large power system.

A. Application to 14-machine Test System

Figure 4 shows a single-line diagram of the 14-machine test system in Australia [38]. The test system consists of 68

buses, 14 generators, and five static var compensators (SVCs), and encompasses the interconnected operation of five coherent regions.
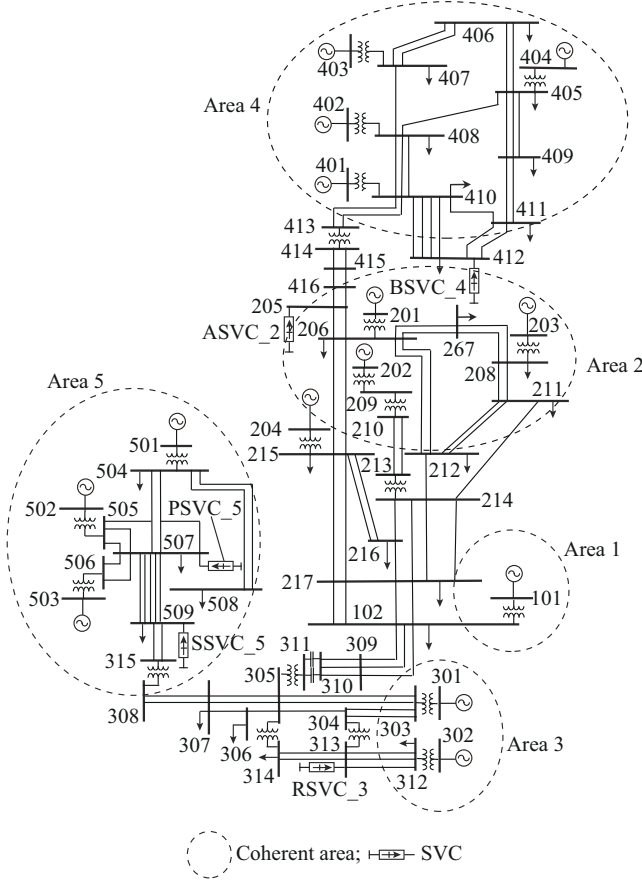

Fig. 4. Single-line diagram of 14-machine test system in Australia.

The time series extracted from transient stability simulations are used to investigate the application of multiblock analysis to extract and characterize system oscillations. As an example, Fig. 5 shows the machine speed deviations of the system generators following a 1% load shedding at bus 217.
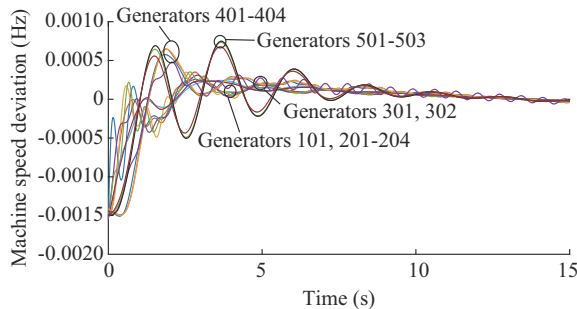

Fig. 5. Machine speed deviations of system generators following a 1% load shedding at bus 217.

In the studies described below, 1503 samples corresponding to an observational window of 30 s are used to generate a 1503×14 measurement space.

On the basis of a coherency analysis, the 14 machine speed signals are divided into five blocks of variables associ-

ated with coherent areas 1-5 in Fig. 4. Table I lists the characteristics of the signals selected for analysis. Since the regression is of no interest here, the output measurement matrix Y is assumed to equal the input measurement matrix X, i.e., $Y=X$.

TABLE I
CHARACTERISTICS OF SIGNALS SELECTED FOR ANALYSIS

Area (data block)	Characteristic
1 (X_1)	1 signal (speed deviation, Generator 101, area 1)
2 (X_2)	4 signals (speed deviations, area 2)
3 (X_3)	2 signals (speed deviations, area 3)
4 (X_4)	4 signals (speed deviations, area 4)
5 (X_5)	3 signals (speed deviations, area 5)

As summarized in Table II, a dynamic mode decomposition (DMD) analysis of the speed deviation signals in Fig. 5 shows a dominant interarea mode at about 0.328 Hz and a high-frequency local mode at about 0.463 Hz. The first swing mode (0.328 Hz) describes an oscillation in which areas 1-3 and 5 swing in opposition to area 4. The second swing mode (0.463 Hz) describes an oscillation in which areas 1-4 swing in opposition to area 5.

TABLE II
DMD ANALYSIS RESULTS OF SPEED DEVIATION SIGNALS IN FIG. 5

Mode	Frequency (Hz)	Damping (%)	Shape
1	0.328	24.86	Areas 1-3, 5 v.s. area 4
2	0.463	11.52	Areas 1-4 v.s. area 5

Two procedures for modal extraction are investigated and tested: ① MB-PCA of the unfolded measurement matrix $X=[X_1, X_2, X_3, X_4, X_5]$; and ② a DMD analysis of X treated as a single block.

Figure 6 compares the multiblock data analysis of the corresponding speed-based mode shape for the dominant mode at about 0.328 Hz. The results are found to be very similar, although some discrepancies are noted.
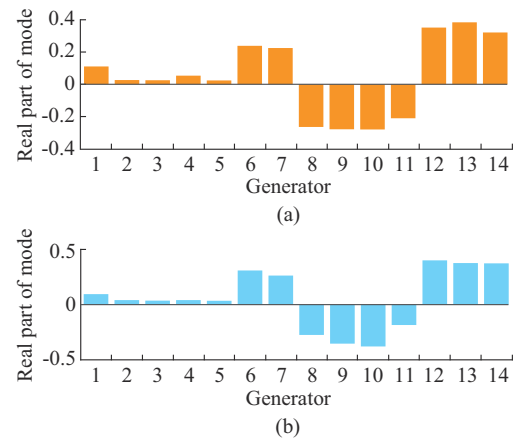

Fig. 6. Multiblock data analysis of corresponding speed-based mode shape for dominant mode at about 0.328 Hz. (a) DMD analysis. (b) MB-PCA.

As a first step, the accuracy of the model is assessed for various contingency scenarios. Numerical results for comparing the performance of the technique are described below.

Figure 7 compares the first two dominant PCs extracted using the SB-PCA and MB-PCA approaches in Table I. The simulation results indicate that both approaches can appropriately characterize the behavior of the system.
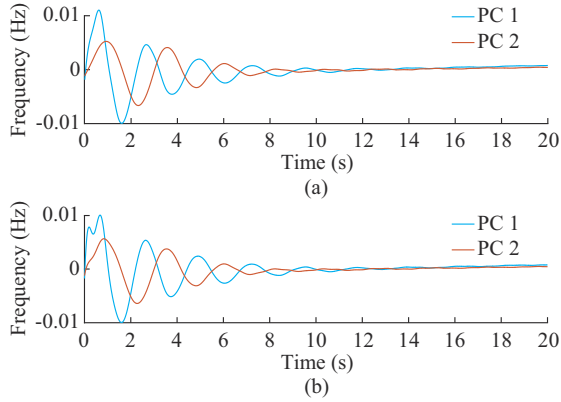

Fig. 7. Comparison of two dominant PCs extracted using SB-PCA and MB-PCA. (a) Single-block model. (b) Multiblock model.

Further insight into the contribution of each regional system to the global system dynamics is obtained from the super-score (block) weights w_i in Fig. 8, where areas 3-5 significantly contribute to the 0.328 Hz interarea mode, while areas 1 and 2 have the least participation in the mode.
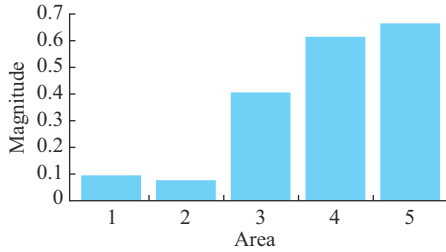

Fig. 8. Block weights w_i in (8) showing contribution of each area to global dynamics for PCA mode 1.

Next, MB-PCA and higher-order PCA are used to assess the impact of wind penetration on the inter-system oscillations. Moreover, the analyses examine the effects of the two data types on the dynamic behavior of power system.

B. Application to 5449-bus 635-generator Equivalent Model of a Large Power System

The developed procedures are further tested on a realistic 5449-bus 635-generator equivalent model of a large power system. Figure 9 depicts the schematic of the system showing the locations of the regional PDCs and the major generators and wind farms (WFs). The equivalent model consists of 5449 buses, 26 WFs, and eight photovoltaic farms representing the operation of seven interconnected areas.

As shown in Fig. 9, each geographic area is assumed to have one PDC, and the information is sent to a super PDC located at the national energy control center. For the clarity of visualization, the data from 40 major generators out of the original 635 generators and 26 WFs are used for the joint analysis of the system behavior. These machines represent the generators and WFs with the most significant participation in the slowest interarea mode.
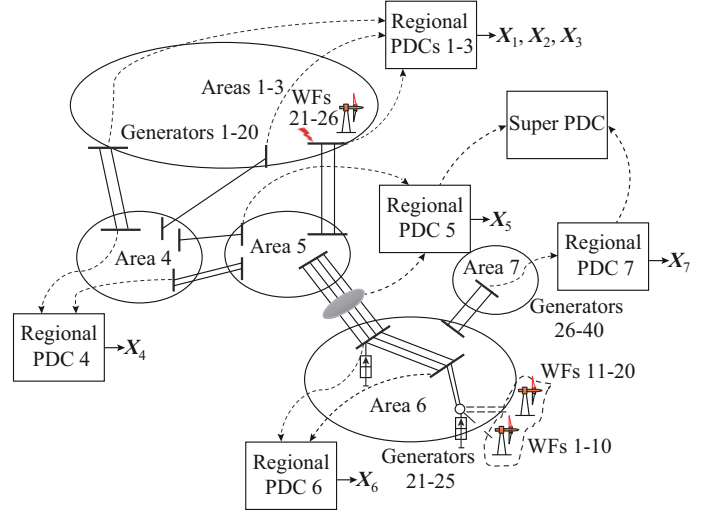

Fig. 9. Schematic of system showing locations of regional PDCs and major generators and WFs.

Detailed simulations of the transient stability have been conducted to generate the observational data in (1). Solutions are obtained using a time step of 5 ms and a time window of 30 s for 1604 samples. Before applying the proposed procedures, data are decimated from the initial rate of 200 Hz to 20 Hz to emulate the actual sampling rate of the PMU used in the system.

A 10 s overlapping window is utilized for screening purposes following the approach in [39], [40].

Five blocks of variables are considered for analysis, including the deviations in both the generator speed and WF speed. Table III summarizes the main characteristics of the signals used in the analyses below.

TABLE III
MAIN CHARACTERISTICS OF SIGNALS USED IN ANALYSES

Area (data block)	Selected signal
1 ($X_{g_{1-3}}$)	20 generator speed signals in areas 1-3
2 (X_{g_6})	5 generator speed signals in area 6
3 (X_{g_7})	15 generator speed signals in area 7
4 (X_{wf_6})	19 WF speed signals in area 6
5 ($X_{wf_{1-3}}$)	7 WF speed signals in areas 1-3

The contingency considered is a three-phase stub fault at the interface between areas 3 and 5. This contingency is found to excite the slowest system mode at about 0.395 Hz. Two main datasets are used for analysis: ① active output power; and ② speed deviations.

The first dataset consists of the measured active output power of the selected generators and WFs in Table III. The second dataset corresponds to speed deviations.

Figure 10 shows the signals selected for multiblock analysis of system behavior, including the WF and generator speeds and active output power, which are simultaneously measured at 66 locations. Nonlinear detrending techniques have been applied to the WF speed deviations before apply-
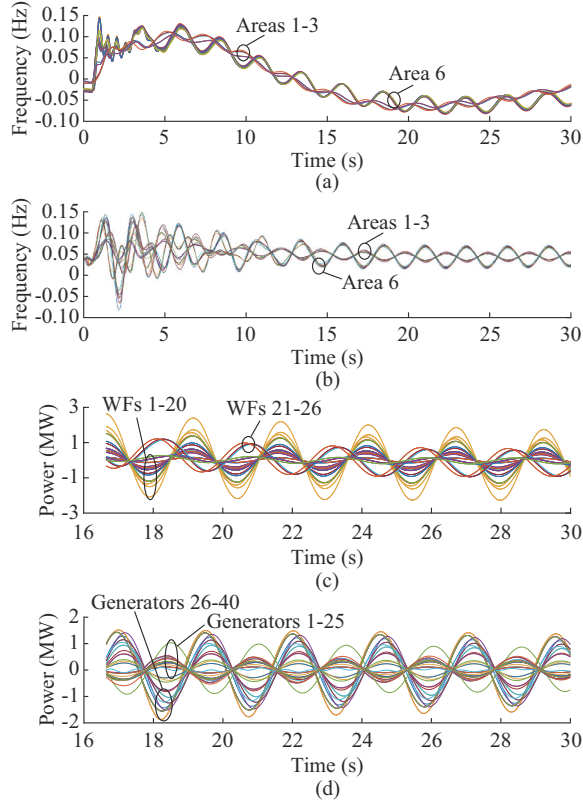
ing MB-PCA [41].

Fig. 10. Signals selected for multiblock analysis of system behavior. (a) WF speed. (b) Generator speed. (c) WF active output power. (d) Generator active output power.

For reference, Tables IV and V list the damping and frequency for the signals in Fig. 10 extracted by using DMD [42], where ξ is the damping ratio. The simulation results reveal a poorly damped mode at about 0.395 Hz associated with the oscillation of machines in areas 1-3. The presence of a strong trend at 0.055 Hz is also noted.

TABLE IV
DMD ANALYSIS RESULTS: ACTIVE OUTPUT POWER DEVIATIONS

Mode	Modal energy (%)	Frequency (Hz)	ξ (%)
1	42.810	0.397	0.490
2	4.530	0.022	44.960
3	0.822	0.792	1.189
4	0.221	0.671	11.480

TABLE V
DMD ANALYSIS RESULTS: SPEED DEVIATIONS

Mode	Modal energy (%)	Frequency (Hz)	ξ (%)
1	24.530	0.395	0.49
2	9.440	0.055	36.03
3	0.193	0.670	9.97
4	0.064	0.791	5.79

On the basis of this discussion, the dataset X in (2) is defined as:

$$X = [X_{g_{1-3}} \quad X_{g_6} \quad X_{g_7} \quad X_{wf_6} \quad X_{wf_{1-3}}] \in \Re^{N \times m_t} \quad (21)$$

where $m_t = 66$; and $N = 1604$.

1) Mode Shapes for MB-PCA

Figure 11 compares the loading (shape or spatial patterns) extracted from MB-PCA in (7) with those obtained using the DMD approach. In these studies, the signals are detrended and centered using the approach in [42]. Numerical experience shows that this approach is more effective for scaling and centering data than standard techniques.
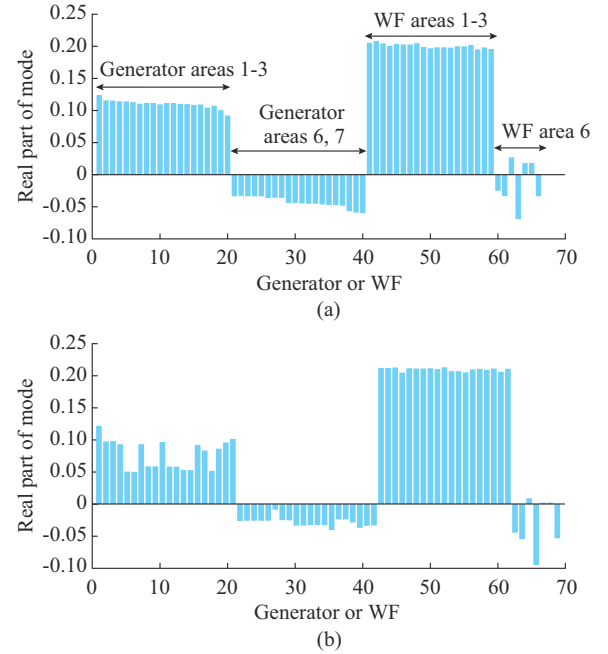

Fig. 11. Comparison of loading (shape or spatial patterns) extracted from MB-PCA in (7) with those obtained using DMD approach. (a) MB-PCA scores for the slowest PCA mode in (9). (b) Speed-based mode shape obtained from a DMD analysis.

As can be observed, the synchronous generators and WFs in areas 6 and 7 swing in opposition to those in areas 1-3. The inconsistent results in Fig. 11 emphasize the importance of properly (nonlinearly) detrending the observation data, especially in the case of large frequency deviations in distributed WFs. A comparison of the numerical results in Fig. 11 shows that MB-PCA adequately represents the inter-system behavior.

The second problem of interest is to determine the machines or states that make the most significant contributions to the slowest interarea mode. After computing the matrix of scores T, the measures of contribution are determined using (13).

The variables (generators/WFs) with the most significant contribution C_r in (13) for each regional system determined using this procedure for each area are Generator 1 (area 1), Generator 2 (area 2), Generator 9 (area 3), WF 3 (data block 4), and WF 6 (data block 5). This information can be used to determine the centers of areas for MB-PLS or to derive the control strategies.

2) Integrated ST-HOSVD Analysis of Multiple Data Types

The data modality poses a particular challenge to the con-

ventional MB-PCA approaches in Section III, as the model dimensionality directly increases with the number of data features. Motivated by this problem, ST-HOSVD is employed to assess the impact of multichannel data on the dynamic behavior of power system.

For illustration, this paper focuses on the joint analysis of the datasets in Fig. 10 (Case 1 in Section IV) in the subsequent discussion. In the ST-HOSVD framework, this representation results in a three-way tensor of dimensions $N \times p \times n_t$ with $p = 2$ data types.

In this case, the data are further subdivided into four blocks. The modified measurement matrix is defined as:

$$X = \left[\underbrace{X_{s_g} \quad X_{s_{wf}}}_{X_1} \quad \underbrace{X_{p_g} \quad X_{p_{wf}}}_{X_2}\right] \tag{22}$$

For clarity of illustration, the measurement subsets in (22) for Tucker tensor analysis are defined in Table VI.

TABLE VI
MEASUREMENT SUBSETS IN (22) FOR TUCKER TENSOR ANALYSIS

Data block	Features
X_{s_g}	40 generator speed signals
$X_{s_{wf}}$	26 WF speed signals
X_{p_g}	40 generator active output power signals
$X_{p_{wf}}$	26 WF active output power signals

From Table VI, the three-way data are arranged into a tensor $\hat{\chi} \in \mathfrak{R}^{n_t \times N \times p}$ with $n_t = 66$, $N = 1604$, and $p = 2$ (two data types). As discussed above, the application of HOSVD allows the three-way observational data to be expressed in terms of a core matrix G and reduced matrix $U^{(1)}$ as shown in (17), where $G \in \mathfrak{R}^{61 \times 1604 \times 2}$, $U^{(1)} \in \mathfrak{R}^{66 \times 61}$, $U^{(2)} \in \mathfrak{R}^{1604 \times 121}$, and $U^{(3)} \in \mathfrak{R}^{2 \times 2}$. Two different problems are of interest here: ① extracting the global oscillation modes from (17); and ② identifying the dominant modes and interaction features by using a Tucker PCA model.

Owing to its analytical nature, HOSVD acts as a filter to single out the dominant (slowest) oscillation mode at about 0.395 Hz. This is illustrated in Fig. 12, which shows the two dominant temporal modes extracted using G in (17) and (19) from the dataset in (22). They correspond to the time evolution of the PCA mode at 0.395 Hz, and the global trend.

Further, Fig. 13 depicts the speed-based mode shape of the speed deviation signals in Fig. 10 obtained using ST-HOSVD. In this analysis, the accuracy criterion ε in (20) is set to be 1×10^{-5}.

The results correlate well with those computed using MB-PCA and the DMD analysis in Fig. 11. For Case 1, the CPU time for the ST-HOSVD approach and MB-PCA is 0.53 s and 1.92 s, respectively.

3) Mode Shapes for MB-PCA

Additional insight into the use of data types is obtained using MB-PCA for the speed deviations and active power deviations in (22). Figure 14 shows the extracted score or shapes for the dominant PC using MB-PCA.
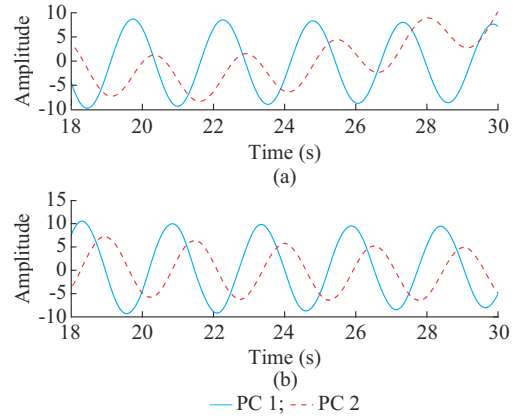

Fig. 12.   Time evolution of modal components extracted using ST-HOSVD submatrices. (a) X_1. (b) X_2.
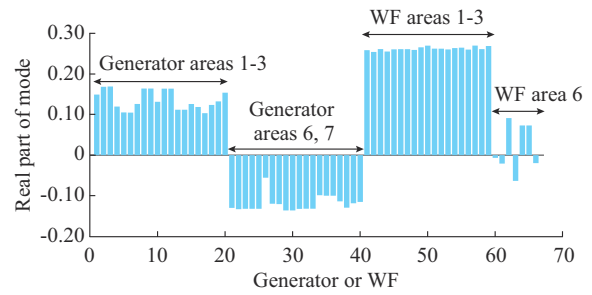

Fig. 13.   Speed-based mode shape of speed deviation signals in Fig. 10 obtained using ST-HOSVD.
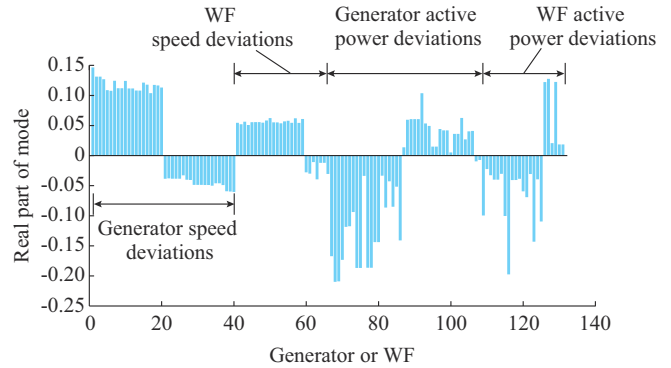

Fig. 14.   Extracted score or shapes for dominant PC using MB-PCA.

From this analysis (Case 2 in Section IV), the participation of blocks from the score weights is found to be 0.5862 (block 1), 0.2542 (block 2), 0.6729 (block 3), and 0.4013 (block 4), indicating that the generator speed deviation and active output power signals (block 3) have the most significant participation in the 0.395 Hz mode.

Moreover, the analysis shows the phase of the modal contribution from various data types in a single plot.

4) Feature-level Modal Analysis

The system monitoring at the modal (feature) level involves combining or integrating temporal scales. Each area is treated as a single data block, and the dominant scales are extracted using any linear or nonlinear modal analysis technique (Case 3 in Section IV). For example, let the measured data in area k be approximated by the DMD model as [39]:

$$\tilde{X}_k \approx \sum_{j=1}^{r_k} \varphi_j \lambda_j a_j^{\mathrm{T}} \qquad (23)$$

where $a_j(t) = [a_j(t_0), a_j(t_1), ..., a_j(t_{N-1})]$ is the jth vector of the temporal amplitudes; φ_j is the dynamic or spatial mode; and λ_j is the associated frequency. The index r_k is the number of significant modes within a frequency band of interest, i. e., $\omega_{\min} \le \omega_j \le \omega_{\max}$ for area k.

The temporal components in (23) are then used to build the feature-based matrix as:

$$\hat{X}_j(t) = \begin{bmatrix} a_1(t_0) & \cdots & a_{r_1}(t_0) & \cdots & a_k(t_0) & \cdots & a_{r_k}(t_0) \\ a_1(t_1) & \cdots & a_{r_1}(t_1) & \cdots & a_k(t_1) & \cdots & a_{r_k}(t_1) \\ \vdots & & \vdots & & \vdots & & \vdots \\ a_1(t_{N-1}) & \cdots & a_{r_1}(t_{N-1}) & \cdots & a_k(t_{N-1}) & \cdots & a_{r_k}(t_{N-1}) \end{bmatrix}$$
$$\underbrace{\qquad\qquad}_{\text{Frequency band 1}} \qquad \underbrace{\qquad\qquad}_{\text{Frequency band } k}$$
$$(24)$$

The dimension of matrix is $N \times r_T$, where $r_T = r_1 + r_2 + ... + r_M$, $r_1 \ne r_2 \ne ... \ne r_M$ in general, i. e., the number of selected modes is allowed to differ.

Similar representations can be obtained using wavelets or other system identification and control modeling techniques [43], [44].

In the first step, the DMD modes associated with a given region or block of variables are obtained using (23); in the second step, the temporal components $a_j(t)$ are combined to yield the overall superblock-level model. Then, regular SB-PCA is applied to the single-block representation, and the measures of association can be estimated using CCA or PCA.

Figure 15 shows the time evolution of the dominant PC modes in Case 3, which are extracted using the above procedure. Here, PC modes 1 and 2 capture the 0.395 Hz sustained oscillation, while PC mode 3 captures the global trend. Again, the results compare well with the HOSVD model in Fig. 12. However, the feature-level modal approach is rather elaborate, and the energy criteria need to be specified to retain the number of significant modes within the frequency band of interest.
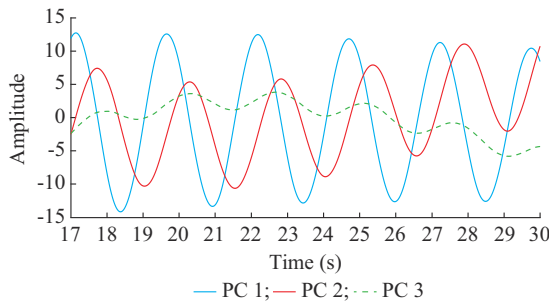

Fig. 15.   Time evolution of dominant PC modes in Case 3.

VI. Conclusion

In this paper, the MB-PCA and ST-HOSVD approaches based on Tucker decomposition are used in a complementary manner to evaluate and characterize the interregional oscillations in hierarchical distributed WAMSs.

The techniques for relating blocks of variables associated with local systems or areas are examined, and the approach-es for analyzing the effect of multiple data types on the system behavior are proposed.

The results demonstrate that multiblock analysis techniques are scalable and efficient for analyzing local and global oscillations in hierarchical distributed WAMSs. This analysis can provide guidelines for selecting variables of interest during the design of WAMSs and control/monitoring strategies and studying the impact of distributed generation on the dynamic behavior of power system.

Efforts to generalize the proposed framework to a tensor representation of multiple heterogeneous datasets are actively investigated. Further, two novel avenues for research are envisaged: ① ST-HOSVD-based PCA; and ② partial least-squares (PLS) analysis and tensor-based sensor placement. In addition, an investigation is necessary to assess the applicability of multiblock analysis techniques to combine or fuse data in near-real-time applications.

References

[1] M. Shahidehpour and Y. Wang, *Communication and Control in Electric Power Systems*, Hoboken: Wiley-IEEE Press, 2003.

[2] S. M. Ali, M. Jawad, B. Khan *et al.*, "Wide area smart grid architectural model and control: a survey," *Renewable and Sustainable Energy Reviews*, vol. 64, pp. 311-318, Oct. 2016.

[3] A. R. Messina, *Wide-area Monitoring of Interconnected Power Systems*, 1st ed., London: IET Press, 2015.

[4] M. Shahraeini, M. H. Javidi, and M. S. Ghazizadeh, "Comparison between communication infrastructure of centralized and decentralized wide area measurement systems," *IEEE Transactions on Smart Grid*, vol. 2, no. 1, pp. 206-211, Mar. 2011.

[5] A. Swinghamer, "Analyze the effects of remote wind generation using synchrophasors," SEL Application note, AN2009-61, 2009, https://cms-cdn. selinc. com//assets/Literature/Publications/Application% 20Notes/AN2009-61_20091020.pdf?v=20150916-203039

[6] P. J. Harding, A. Varghese, R. Bharat *et al.*, "Implementation of a wide-area monitoring scheme for the Indian power system," in *Proceedings of the 13th International Conference on Development in Power System Protection (DPSP)*, Edinburgh, UK, Mar. 2016, pp. 1-9.

[7] L. Wang, "Dynamic reduction of large power systems for stability studies," *IEEE Transactions on Power Systems*, vol. 12, no. 2, pp. 889-895, May 1997.

[8] X. Zhang, Y. Xue, S. You *et al.*, "U. S. eastern interconnection (EI) model reductions using a measurement-based approach," in *Proceedings of the 2018 IEEE/PES Transmission and Distribution Conference and Exposition (T&D)*, Denver, USA, Apr. 2018, pp. 1-5.

[9] S. Nabavi, J. Zhang, and A. Chakrabortty, "Distributed optimization algorithms for wide-area oscillation monitoring in power systems using interregional PMU-PDC architectures," *IEEE Transactions on Smart Grid*, vol. 6, no. 5, pp. 2529-2538, Sept. 2015.

[10] J. Zhang, M. Weiss, A. Chakrabortty *et al.*, "ExoGENI-WAMS: a cyber-physical testbed for wide-area monitoring and control of power systems using distributed cloud computing," in *Proceedings of the International Synchrophasor Symposium*, Atlanta, USA, Mar. 2015, pp. 1-22.

[11] M. Warnier, S. Dulman, Y. Koç *et al.*, "Distributed monitoring for the prevention of cascading failures in operational power grids," in *Proceedings of the International Journal of Critical Infrastructure Protection*, vol. 17, pp. 15-27, Jun. 2017.

[12] A. R. Messina, *Data Mining and Data Fusion for Power System Monitoring*, Boca Ratón: CRC Press, 2020.

[13] I. R. Cabrera, E. Barocio, R. J. Betancourt *et al.*, "A semi-distributed energy-based framework for the analysis and visualization of power system disturbances," *Electric Power Systems Research*, vol. 143, pp. 339-346, Feb. 2017.

[14] G. A. Taylor, M. R. Irving, P. R. Hobson *et al.*, "Distributed monitoring and control of future power systems via grid computing," in *Proceedings of the 2006 IEEE PES General Meeting*, Montreal, Canada, Jun. 2006, pp. 1-5.

[15] C. Tong and X. Yan, "A novel decentralized process monitoring scheme using a modified multiblock PCA algorithm," *IEEE Transac-*

tions on Automation Science and Engineering, vol. 14, no. 2, pp. 1129-1138, Apr. 2017.

[16] J. A. Westerhuis, T. Kourti, and J. F. Macgregor, "Analysis of multi-block and hierarchical PCA and PLS models," *Journal of Chemometrics*, vol. 12, pp. 301-321, Sept.-Oct. 1998.

[17] A. K. Smilde, J. A. Westerhuis, and S. de Jong, "A framework for sequential multiblock component methods," *Journal of Chemometrics*, vol. 17, pp. 323-337, Jun. 2003.

[18] Q. Jiang and X. Yan, "Dynamic CCA-based distributed monitoring for multiunit non-Gaussian processes," *IFAC-PapersOnLine*, vol. 51, no. 21, pp. 1-6, Aug. 2011.

[19] S. Unkel, A. Hannachi, N. T. Trindafilov *et al.*, "Independent component analysis for three-way data with an application from atmospheric science," *Journal of Agricultural, Biological, and Environmental Statistics*, vol. 16, no. 3, pp. 319-338, Sept. 2011.

[20] Y. Zhang, G. Zhou, J. Jin *et al.*, "L_1-regularized multiway canonical correlation analysis for SSVEP-based BC," *IEEE Transactions on Neural System Rehabilitation*, vol. 21, no. 6, pp. 887-896, Nov. 2013.

[21] X. Zhuang, Z. Yang, and D. Cordes, "A technical review of canonical correlation analysis for neuroscience applications," *Human Brain Mapping*, vol. 41, pp. 3807-3822, Sept. 2020.

[22] S. Wold, N. Kettaneh, and K. Tjessem, "Hierarchical multiblock PLS and PC models for easier interpretation and as an alternative to variable selection," *Journal of Chemometrics*, vol. 99, pp. 463-482, Sept.-Dec. 1992.

[23] J. A. Westerhuis and P. M. Coenegracht, "Multivariate modeling of the pharmaceutical two-step process of wet granulation and tableting with multiblock partial least squares," *Journal of Chemometrics*, vol. 11, no. 5, pp. 379-392, Sept. 1997.

[24] A. R. Messina and V. Vittal, "Extraction of dynamic patterns from wide-area measurements using empirical orthogonal functions," *IEEE Transactions on Power Systems*, vol. 22, no. 2, pp. 682-692, May 2007.

[25] G. Kerschen, J. Golinval, A. F. Vakakis *et al.*, "The method of proper orthogonal decomposition for dynamical characterization and order reduction of mechanical systems: an overview," *Nonlinear Dynamics*, vol. 41, pp. 147-169, 41, Aug. 2005.

[26] S. J. Qin, S. Valle, and M. J. Piovoso, "On unifying multiblock analysis with application to multiblock process monitoring," *Journal of Chemometrics*, vol. 15, pp. 715-742, Aug. 2001.

[27] Y. Xu and R. Goodacre, "Multiblock principal component analysis: an efficient tool for analyzing metabolomics data which contain two influential factors," *Metabolonomics*, vol. 8, pp. 37-51, Sept. 2012.

[28] B. Worley and R. Powers, "A sequential algorithm for multiblock orthogonal projections to latent structures," *Chemometric Intelligent Laboratory Systems*, vol. 149, pp. 33-39, Dec. 2015.

[29] S. Bougeard, E. M. Qannarib, and N. Rose, "Multiblock redundancy analysis: interpretation tools and application in epidemiology," *Journal of Chemometrics*, vol. 25, pp. 467-475, Apr. 2011.

[30] M. Tenenhaus, A. Tenenhaus, and P. J. F. Groenen, "Regularized generalized canonical correlation analysis: a framework for sequential multiblock component methods," *Psychometrika*, vol. 82, no. 3, pp. 737-777, May 2017.

[31] T. G. Kolda and B. W. Bader, "Tensor decompositions and applications," *SIAM Review*, vol. 51, no. 3, pp. 455-500, Aug. 2009.

[32] H. Kolla, K. Aditya, and J. H. Chen, "Higher order tensors for combustion data analysis and compression," Sandia National Laboratories, Albuquerque, USA, Tech. Rep. SAND2019-12585B680508, Oct. 2019.

[33] N. D. Sidiropoulous, L. D. Lathauwer, X. Fu *et al.*, "Tensor decomposition for signal processing and machine learning," *IEEE Transactions on Signal Processing*, vol. 65, no. 3, pp. 3551-3582, Jul. 2017.

[34] Z. Zhang, G. I. Allen, H. Zhu *et al.*, "Tensor network factorizations: relationships between brain structural connectomes and traits," *Neuroimage*, vol. 197, pp. 330-343, Aug. 2019.

[35] L. de Lathauwer, B. de Moor, and J. Vandewalle, "A multilinear singular value decomposition," *SIAM Journal of Matrix Analysis and Applications*, vol. 21, pp. 1253-1278, Jan. 2000.

[36] Z. Fang, X. Yang, L. Han *et al.*, "A sequentially truncated higher-order singular value decomposition-based algorithm for tensor completion," *IEEE Transactions on Cybernetics*, vol. 49, no. 5, pp. 1956-1967, May, 2019.

[37] N. Vannieuwenhoven, R. Vandebril, and K. Meerbergen, "A new truncation strategy for the higher-order singular value decomposition," *SIAM Journal of Scientific Computation*, vol. 34, no. 2, pp. 1027-1052, Mar.-Apr. 2012.

[38] C. Cañizares, T. Fernandes, E. Geraldi Jr. *et al.*, "Benchmark models for the analysis and control of small-signal oscillatory dynamics in

power systems," *IEEE Transactions on Power Systems,* vol. 32, no. 1, pp. 715-722, Jan. 2017.

[39] A. Allen, S. Santoso, and E. Muljadi, "Algorithm for screening phasor measurement unit data for power system events and categories and common characteristics for events seen in phasor measurement unit relative phase-angle differences and frequency signals," National Renewable Energy Laboratory, Golden, USA, Tech. Rep. NREL/TP-5500-58611, Aug. 2013.

[40] O. P. Dahal and S. M. Brahma, "Preliminary work to classify the disturbance events recorded by phasor measurement units," in *Proceedings of the 2012 IEEE PES General Meeting*, San Diego, USA, Jul. 2012, pp. 1-8.

[41] A. R. Messina, V. Vittal, G. T. Heydt *et al.*, "Nonstationary approaches to trend identification and denoising of measured power system oscillations," *IEEE Transactions on Power Systems*, vol. 24, no. 4, pp. 1798-1807, Nov. 2009.

[42] E. Barocio, B. C. Pal, N. F. Thornhill *et al.*, "A dynamic mode decomposition framework for global power system oscillation analysis," *IEEE Transactions on Power Systems*, vol. 30, no. 6, pp. 2906-2913, Nov. 2015.

[43] C. M. Rergis, I. Kamwa, R. Khazaka *et al.*, "A Loewner interpolation method for power system identification and order reduction," *IEEE Transactions on Power Systems*, vol. 34, no. 3, pp. 1834-1844, May 2019.

[44] B. R. Bakshi, "Multiscale PCA with application to multivariate statistical process monitoring," *AIChE Journal Process Engineering*, vol. 44, no. 7, pp. 1596-1610, Jul. 1998.

Arturo Román-Messina received the M.Sc. degree (with Hons.) in electrical engineering from the National Polytechnic Institute of Mexico, Mexico City, Mexico, in 1987, and the Ph.D. degree from Imperial College, London, UK, in 1991. Since 1997, he has been a Professor in the Center for Research and Advanced Studies (CINVESTAV), Guadalajara, Mexico. His research interests include power system stability analysis and control, and development and application of measurement-based signal processing techniques to study transient processes in power systems.

Alejandro Castillo-Tapia received the B.E. degree in communications and electronics engineering from the National Polytechnic Institute, Mexico City, Mexico, in 2000, and the M.Sc. degree in Electrical Engineering from Center for Research and Advanced Studies of the National Polytechnic Institute (CINVESTAV-IPN), Mexico City, Mexico, in 2003. He is currently pursuing his Ph.D. degree in electrical engineering at CINVESTAV, Guadalajara, Mexico. His research interests include power system state estimation and optimal sensor placement.

David A. Román-Garcíais currently pursuing the B.Sc. degree in engineering physics at Tecnológico de Monterrey, Monterrey, Mexico. His research interests include scattering control in photonic lattices, waveguide quantum electrodynamics (WQED) analogies, and numerical modeling.

Marcos A. Hernández-Ortega received the M.Sc. and the Ph.D. degrees in electrical engineering from Center for Research and Advanced Studies (CINVESTAV), Guadalajara, Mexico, in 2014 and 2019, respectively. Currently, he is a researcher at the Electromechanical Engineering Department of the Universidad Autónoma de Guadalajara (UAG), Guadalajara, Mexico. His research interests include dynamical analysis of nonlinear systems and extraction and identification of nonlinear patterns from measurements.

Carlos A. Morales-Rergis received the M.Sc. and Ph.D. degrees in electrical engineering from Center for Research and Advanced Studies (CINVESTAV), Guadalajara, Mexico, in 2014 and 2019, respectively. He was a Research Assistant with CINVESTAV. Currently, he is with the Research Department of the Center for Industrial and Technical Studies (CETI) and with UAG, Guadalajara, Mexico. His research interests include extraction of dominant subspaces for identification and order reduction of power systems models.

Claudia M. Castro Arvizu received the B.E. degree from University of Guanajuato, Guanajuato, Mexico, in 2013, the M.Sc. and Ph.D. degrees in electrical engineering from Center for Research and Advanced Studies (CINVESTAV), Guadalajara, Mexico, in 2015 and 2020, respectively. She is currently with the Department of Design, Science, and Technology, UAG, Mexico. Her research interests include power system dynamics, computational intelligence, and data mining.